Supporting Information

Migration-mitigated crossover of organic redox anion across proton-exchange membrane

Penghui Ding[1], Mikhail Vagin[1,2]*, Mohammad Javad Jafari[4], Aleksandar Y. Mehandzhiyski[1], Viktor Gueskine[1,3], Tobias Abrahamsson[1], Igor Zozoulenko[1,3], Thomas Ederth[4], Reverant Crispin[1,2,3]

[1]Laboratory of Organic Electronics, Department of Science and Technology, Linköping University, 60174 Norrköping, Sweden

[2]Wallenberg Initiative Materials Science for Sustainability, Department of Science and Technology, Linköping University, Norrköping 60174, Sweden

[3]Wallenberg Wood Science Center, Linköping University, 60174 Norrköping, Sweden

[4]Department of Physics, Chemistry and Biology, Linköping University, 58183 Linköping, Sweden,

*Corresponding author: mikhail.vagin@liu.se, +46702753087

Supporting Note 1.

Geometry of the system and governing equations for the modelling part

To model the flux of species across the membrane and the device, we created 1D model based on the generalized Poisson-Nernst-Planck equations. The model consists of two porous electrode domains (anode and cathode) and a membrane domain placed in-between the two electrodes and depicted in Figure 1A. The anode and cathode consist of solid (carbon felt) and liquid (electrolyte) phases with volume fractions 0.1 and 0.9, respectively. In our model, the cathode electrolyte contains $i_{cathode} = H^+, HSO_4^-, SO^{2-}_4, O_2$ and the anode electrolyte contains $i_{anode} = H^+, HSO_4^-, SO^{2-}_4, Tiron^{2-}$ species.

The transport of species is governed by the mass balance equation:

$$\frac{\partial c_i}{\partial t} + \nabla \cdot J_i + u \cdot \nabla c_i = R_{i,tot} \#(1)$$

where $R_{i,tot}$ is the total reaction rate of the species i; u denotes the flow rate. $R_{i,tot}$ has contributions from Faradaic reactions R_F and acid dissociation R_d:

$$R_{i,tot} = \sum_i R_{F,i} + R_{d,i} \#(2)$$

J_i represents the flux density of species i due to diffusion and migration:

$$J_i = - D_i \nabla c_i - z_i \mu_i F c_i \nabla \varphi_l \#(3)$$

where D_i is the diffusion coefficient of species i; $\mu_i$denotes its mobility; F is the Faraday constant; φ_l is the electrolyte potential. The mobility μ_i of species i can be computed based on the diffusion coefficient according to: $\mu_i = \frac{D_i}{RT}$, where R is the molar gas constant and T is the temperature. Both equations Eq. (1) and Eq. (2) apply to the membrane and electrodes.

The Nernst-Planck equations Eq. (1)-(2) are coupled with the Poisson equation:

$$- \varepsilon_r \varepsilon_0 \nabla \phi_l = F \sum_i z_i c_i \ \#(4)$$

where ε_0 is the permittivity of vacuum, and $\varepsilon_r = 80$ is the dielectric constant of the electrolyte. The total current in the porous electrodes, i_{tot}, consists of the electrolyte current (i_l) due to the movement of ionic species in the electrolyte phase of the electrode, and the electrode current due to electron transport in the solid carbon felt phase of electrode,

$$i_{tot} = i_l + i_s \quad \#(5)$$

The electrolyte current is given by:

$$i_l = F\sum_{i=1}^{n} z_i J_i \quad \#(6)$$

where J_i represents the flux density of species i due to diffusion and migration. The electrode current (i_s) is computed by:

$$i_s = -\sigma_s \nabla \varphi_s \quad \#(7)$$

where σ_s is the conductivity of the porous electrode; φ_s represents the potential in the solid carbon materials.

In the current model the reaction term ($R_{i,tot}$) in the continuity equation (1) accounts only for the dissociation reaction rates of H_2SO_4 species, where the first step of this dissociation reaction is assumed to be fully completed (i.e., $H_2SO_4 \rightarrow H^+ + HSO_4^-$). The $Tiron^{2-}$ oxidation and O_2 reduction are not included in the present model and therefore $R_{F,i} = 0$. We plan to account for these reactions in a follow-up work. The second step of the dissociation reaction (i.e., $HSO_4^- \leftrightarrow SO_4^{2-} + H^+$) is described by the dissociation source term ($R_{d,i}$), and is given by [1]:

$$R_{d,i} = k_d \times \left(\frac{c_{H^+} - c_{HSO_4^-}}{c_{H^+} + c_{HSO_4^-}} - \beta \right) \quad \#(8)$$

where k_d is the coefficient of dissociation reaction; c_{H^+} and $c_{HSO_4^-}$ are the concentration of H^+ and HSO_4^- species; β is the degree of dissociation, where $R_{d,H^+} = -R_d, R_{d,HSO_4^-} = R_d, R_{d,SO_4^{2-}} = -R_d$.

The membrane is modeled with fixed charge distribution of $\rho_{fix} = 1.5$ M negative charges corresponding to the charge density in the experiments. To keep the electroneutrality of the membrane we specified also 1.5 M H^+ as the initial concentration condition in the membrane domain. All species are able to cross the membrane, but their initial concentrations in the membrane were set to 0, except for H^+ as described above. It should be noted that the dissociation $H_2SO_4 \rightarrow H^+ + HSO_4^-$ is suppressed by the presence of the fixed charge in the membrane, and therefore it is excluded from this domain [2].

[1] K.W. Knehr, E. Agar, C.R. Dennison, A.R. Kalidindi, E.C. Kumbur, A transient vanadium flow battery model incorporating vanadium crossover and water transport through the membrane. Journal of The Electrochemical Society 159(9) 2012 A1446–A1459.
[2] G. Pourcelly, A. Lindheimer, C. Gavach, H.D. Hurwitz, Electrical transport of sulphuric acid in nation perfluorosulphonic membranes. Journal of Electroanalytical Chemistry and Interfacial Electrochemistry 305(1) 1991 97–113.

Supporting Note 2.

Tiron quantification by UV-vis

The calibration line of tiron dissolved in DI water (or 1 M H_2SO_4) was obtained by UV–visible spectroscopy with different concentrations (1 mM, 2 mM, 5 mM, 10 mM, 15 mM, and 20 mM). The wavelength of the characteristic maximum absorbance of the two cases (Fig. S1a, c), λ_{max}, is the same 208 nm, which agrees with the literature [1]. Apart from the characteristic peak, the UV-vis spectra also have another two small peaks at 232 and 291 nm [2]. We could obtain the calibration curves for both cases from the absorbance values of known concentrations with a $R^2 > 0.999$, indicating good linearity of the curves. It should be noted that the calibration curves remain nearly the same under different pH.

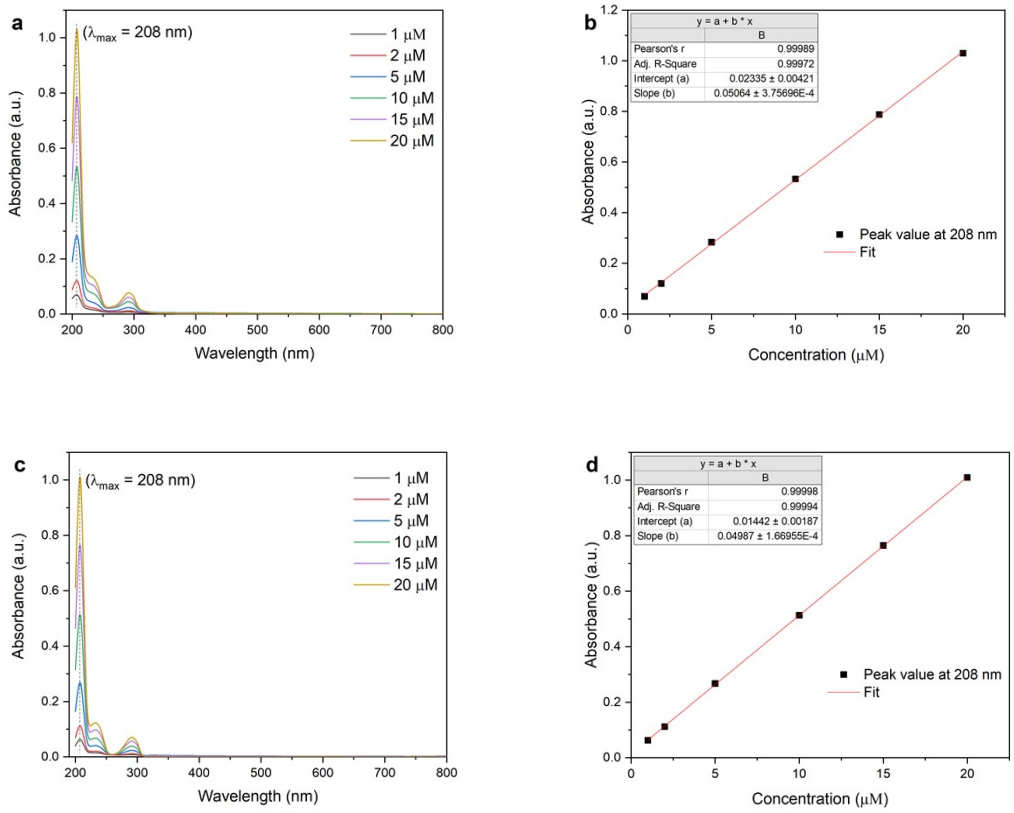

Figure S1. (a, c) UV-vis spectra and (b, d) calibration curves for tiron dissolved in DI water and 1 M H_2SO_4

[1] L. Luo, L. Hou, Y. Liu, K. Wu, Y. Zhu, H. Lu, B. Liang, Regeneration of Na_2Q in an electrochemical CO_2 capture system. Energy Fuels 35(15) (2021) 12260-12269.

[2] S.V. Modak, W. Shen, S. Singh, D. Herrera, F. Oudeif, B.R. Goldsmith, X. Huan, D.G. Kwabi, Understanding capacity fade in organic redox-flow batteries by combining spectroscopy with statistical inference techniques. Nature Communications 14 (2023) 3602.

Supporting Note 3.

Ex-situ ATR-FTIR study in absence of electrolysis

A. Nafion 115 membrane

The set of bands assigned to Nafion was observed for dried Nafion 115 (dried for 45 minutes at 40 ^{o}C) and exposed for 5 minutes either to pure water or to tiron solution in 1 M H_2SO_4 (Fig. S2A-C). As shown in Fig. S2C, a broad band at approximately 3480 cm^{-1} (shifted to around 3420 cm-1 in the wet samples) with a shoulder at 3230 cm^{-1} is attributed to OH stretching, while the band at 1635 cm^{-1} corresponds to HOH bending (Fig. S2B). Notably, these three bands exhibited a substantial increase, around 6-8 times higher, in the wet samples compared to the dry samples (Fig. S2D). The band at 1739 cm^{-1} arises from the bending vibrations of protonated water ($(H2O)_nH^+$) [1, 2], and it is clearly distinguishable from the peak at 1635 cm^{-1}. Importantly, this band signifies the hydrated state and the complete dissociation of sulfonic acid groups, resulting in the release of hydrated protons (as observed in the water wet sample). In the case of the tiron wet sample, the intensity of this band exhibited a more significant increase, approximately 10 times greater, compared to the water wet sample (where most protons are coupled with water molecules). As expected, when Nafion is exposed to 1 M H_2SO_4 FTIR confirms high concentration of protons inside this cation exchanger.

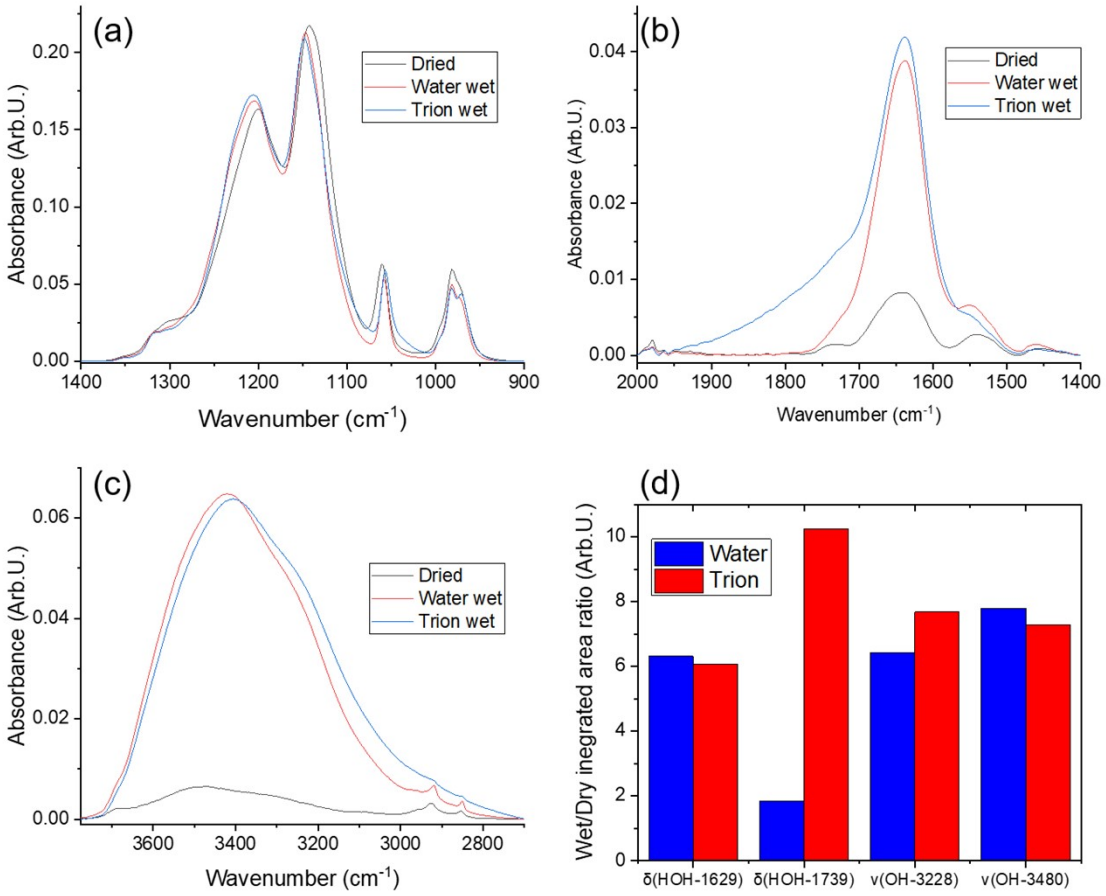

Figure S2. (A-C) ATR-FTIR spectra of water acquired *ex-situ* on dried Nafion 115 (dried for 45 minutes at 40 °C) and exposed for 5 minutes either to pure water or to tiron solution in 1 M H_2SO_4 and (D) integrated area ratios of wet/dry Nafion OH bands. Integrated areas obtained by spectral fitting of overlapped bands. Note: ν: stretching vibration, δ: bending vibration

Table S1. Assignment of observed bands to molecular vibrations in Nafion [3-10]

Assignment	Dried	water wet	tiron wet
C-O-C ether I linkage	971	971	971
C-O-C ether II linkage	981	981	981
Symmetric SO_3 stretching	1061	1058	1056
Symmetric CF_2 stretching	1142	1147	1148
Asymmetric CF_2 stretching	1200	1205	1207
Asymmetric SO_3 stretching	1306	1306	1298
Symmetric C-C stretching	1319	1319	1319
HOH bending (water)	1635	1634	1634
$(HOH)_nH^+$ bending	1739	1736	1735
OH stretching	3228,	3223,	3220, 3409

	3480	3423	

[1] Shimoaka, T., et al., Hydration structure of strongly bound water on the sulfonic acid group in a Nafion membrane studied by infrared spectroscopy and quantum chemical calculation, Physical Chemistry Chemical Physics 17(14) (2015) 8843-8849.

[2] Hallinan, D.T., et al., Diffusion of water in Nafion using time-resolved fourier transform infrared-attenuated total reflectance spectroscopy, Journal of Physical Chemistry B 113(13) (2009) 4257-4266.

[3] Buzzoni, R., et al., Interaction of H2O, CH3OH, (CH3)2O, CH3CN, and Pyridine with the Superacid Perfluorosulfonic Membrane Nafion: An IR and Raman Study. The Journal of Physical Chemistry, 1995. **99**(31): p. 11937-11951.

[4] Gruger, A., et al., Nanostructure of Nafion® membranes at different states of hydration: An IR and Raman study. Vibrational Spectroscopy, 2001. **26**(2): p. 215-225.

[5] Kunimatsu, K., et al., ATR-FTIR Study of Water in Nafion Membrane Combined with Proton Conductivity Measurements during Hydration/Dehydration Cycle. The Journal of Physical Chemistry B, 2011. **115**(15): p. 4315-4321.

[6] Chu, D., et al., Infrared reflectance absorption spectroscopy (IRRAS). Study of the thermal stability of perfluorinated sulphonic acid ionomers on Pt. Journal of Applied Electrochemistry, 1990. **20**(1): p. 157-162.

[7] Shimoaka, T., et al., Hydration structure of strongly bound water on the sulfonic acid group in a Nafion membrane studied by infrared spectroscopy and quantum chemical calculation. Physical Chemistry Chemical Physics, 2015. **17**(14): p. 8843-8849.

[8] Hallinan, D.T., Jr. and Y.A. Elabd, Diffusion of Water in Nafion Using Time-Resolved Fourier Transform Infrared−Attenuated Total Reflectance Spectroscopy. The Journal of Physical Chemistry B, 2009. **113**(13): p. 4257-4266.

[9] Hambardzumyan, A., et al., Nafion membranes reinforced by cellulose nanocrystals for fuel cell applications: aspect ratio and heat treatment effects on physical properties. Journal of Materials Science, 2022. **57**(7): p. 4684-4703.

[10] Cable, K.M., K.A. Mauritz, and R.B. Moore, Effects of hydrophilic and hydrophobic counterions on the Coulombic interactions in perfluorosulfonate ionomers. Journal of Polymer Science Part B: Polymer Physics, 1995. **33**(7): p. 1065-1072.

B. Pure tiron powder

The ATR-FTIR spectrum of pure tiron powder (Fig. SX) shows the presence of the peak at 3543 cm^{-1}, which is attributed to the presence of hydrated Na^+ ions bound water molecules [1-4]. The bands at 3488 and 3250 cm^{-1} arise due to a superposition of asymmetrical and symmetrical vibrations of water, respectively [1, 5], while the HOH bending peak of water appears at 1635 cm^{-1}. The asymmetric and symmetric SO_2 vibration of sulfonate group appear at 1378 and 1186 cm^{-1}, respectively, with a SO_2 bending vibration at 649 cm^{-1} [6-8]. The peaks at 1103 and 1042 are due to S-O bending and stretching of sulfonate group [8-10]. Peaks at 1634, 1588 and 1511 cm^{-1} correspond to the aromatic ring skeletal vibrations, which are combined with C-H deformations (1469, 1435 and 1378 cm^{-1}) and C-C and C-O vibrations (1290, 1223 and 1105 cm^{-1}) [10, 11]. The peak at 3082 cm^{-1} is related to C-H stretching vibration, and the other band between 952-649 cm^{-1} are due to different C-H aromatic ring vibrations [10, 11].

[1] Netskina, O.V., et al., Solid-State NaBH4 Composites as Hydrogen Generation Material: Effect of Thermal Treatment of a Catalyst Precursor on the Hydrogen Generation Rate. Catalysts, 2020. **10**(2): p. 201.

[2] Miller, D.J. and J.M. Lisy, Hydrated Alkali-Metal Cations: Infrared Spectroscopy and ab Initio Calculations of M+(H2O)x=2−5Ar cluster ions for M = Li, Na, K, and Cs. Journal of the American Chemical Society, 2008. **130**(46): p. 15381-15392.

[3] Wang, P., et al., Hydrated Sodium Ion Clusters [Na+(H2O)n (n = 1–6)]: An ab initio Study on Structures and Non-covalent Interaction. Frontiers in Chemistry, 2019. **7**.

[4] Quezado, S., J.C. Kwak, and M. Falk, An infrared study of water–ion interactions in perfluorosulfonate (Nafion) membranes. Canadian journal of chemistry, 1984. **62**(5): p. 958-966.

[5] Panuszko, A., et al., Characteristics of hydration water around hen egg lysozyme as the protein model in aqueous solution. FTIR spectroscopy and molecular dynamics simulation. Physical Chemistry Chemical Physics, 2012. **14**(45): p. 15765-15773.

[6] Philip, D., A. Eapen, and G. Aruldhas, Vibrational and surface enhanced raman scattering spectra of sulfamic acid. Journal of Solid State Chemistry, 1995. **116**(2): p. 217-223.

[7] Roeges, N.P. and J. Baas, A guide to the complete interpretation of infrared spectra of organic structures. 1994: Wiley New York.

[8] Detoni, S. and D. Hadzi, Infra-red spectra of some organic sulphur-oxygen compounds. Spectrochimica Acta, 1956. **11**: p. 601-608.

[9] Chackalackal, S.M. and F.E. Stafford, Infrared Spectra of Methane-, Fluoro-, and Chlorosulfonic Acids. Journal of the American Chemical Society, 1966. **88**(21): p. 4815-4819.

[10] Panicker, C.Y., et al., FT-IR, FT-Raman and SERS spectra of pyridine-3-sulfonic acid. Spectrochimica Acta Part A: Molecular and Biomolecular Spectroscopy, 2006. **64**(3): p. 744-747.
[11] Ajjan, F., et al., Spectroelectrochemical investigation of redox states in a polypyrrole/lignin composite electrode material. Journal of Materials Chemistry A, 2015. **3**(24): p. 12927-12937.

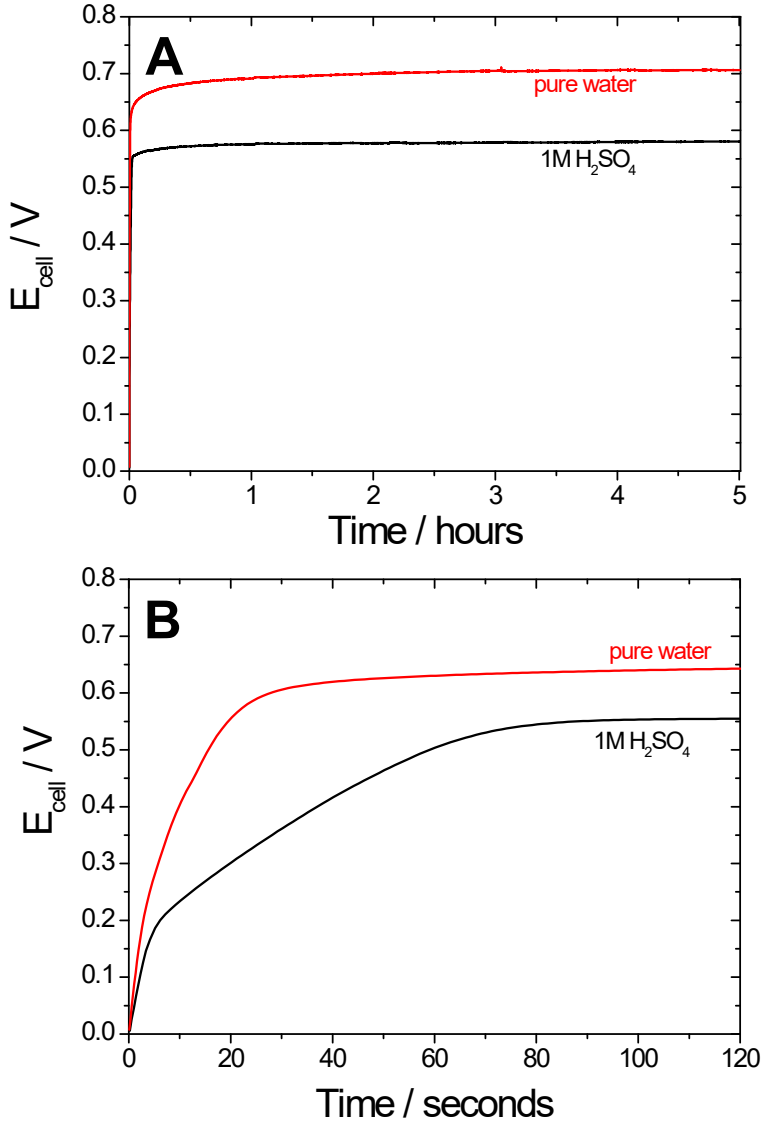

Figure S3. The dynamics of electrolyzer cell voltage upon the application of the electrolysis current (0.08 mA cm^{-2}) at long- and short-time domains (**A** and **B**, respectively).

Table S2. The comparison of performance characteristics of ORR-to-H_2O_2 electrolyzers based on auxiliary oxidation of organics.

Reagent in oxidation process	Cathodic/anodic catalysts	Electrolyte feed	Hydrogen peroxide yield	Faradaic Efficiency, %	Reference
tiron	PEDOT:PSS/No catalyst	1M H_2SO_4 pure water	0.06 mol g^{-1} h^{-1} 0.03 mol g^{-1} h^{-1}	50 20	This work
furfural	Bifunctional TS-1@Co–N–C on nickel foam	0.1M H_2SO_4	6 mmol/L	60	[1]
ethylene glycol	B/N-onion carbon/ Ni_1Mn_1-MOF-Se/NF	1 M KOH	2.48 mmol cm^{-2} h^{-1}	95	[2]
ethylene glycol	Ni-SAC/ Au/$Ni(OH)_2$	0.1M KOH	0.73 mol g^{-1} h^{-1}	85	[3]
furfural	oxidized CNTs/KI	0.1M KOH	9 mmol/L	90	[4]

[1] S.T. Wu, H.L. Zhang, X. Huang, Z.D. Wei, Coupling electrochemical H2O2 production and the in situ selective oxidation of organics over a bifunctional TS-1@Co-N-C catalyst, Chemical Communications 58(64) (2022) 8942-8945.

[2] J. Qi, Y. Du, Q. Yang, N. Jiang, J. Li, Y. Ma, Y. Ma, X. Zhao, J. Qiu, Energy-saving and product-oriented hydrogen peroxide electrosynthesis enabled by electrochemistry pairing and product engineering, Nature Communications 14(1) (2023) 6263.

[3] Y. Sun, K. Fan, J. Li, L. Wang, Y. Yang, Z. Li, M. Shao, X. Duan, Boosting electrochemical oxygen reduction to hydrogen peroxide coupled with organic oxidation, Nature Communications 15(1) (2024) 6098.

[4] X.X. Li, L.C. Cong, H.B. Lin, F.B. Liu, X.X. Fu, H.C. Xu, N. Lin, Linear paired electrolysis of furfural to furoic acid at both anode and cathode in a multiple redox mediated system, Green Energy & Environment 9(1) (2024) 104-113.

Supporting Note 4.

^{1}H-NMR quantification of tiron oxidation in anode compartment

Ex-situ study of tiron oxidation in anode compartment of electrolyzer filled with pure water under constant current electrolysis was done by ^{1}H-NMR. The doublet at 7.34 ppm (J = 2.2 Hz, 1H) in the spectra [1] (Fig. S4) was used to calculate the concentration of tiron (Fig. S5A). The decrease of tiron concentration with elapsed time of electrolysis illustrates the proceeding of anode process. Importantly, the measured concentrations tiron were signfigicantly lower than the predicted by Faraday's law from the electrical charge passed with an assumption of strictly bi-electronic oxidation. Coherently, measured concentrations of oxidation products were smaller than predicted. This illustrates the complex behavior of electrolyzer fed with pure water under conditions of electrolysis at constant current. Specifically, the location of oxidation at anode at narrow 2D region of direct contact of PEM and electrode results in high volumetric current densities, which can cause the complex background processes.

The presence of the new tiron-associated species and the evolution of their concentrations with time of electrolysis (Fig. S5B) illustrate the proceeding of the subsequent electrochemistry-free chemical reaction of oxidized form of tiron with water, namely 1,4 Michael addition reaction (Scheme S1). The products of the Michael addition are available for the subsequent oxidation via at least two additional electrons, which is illustrated by the time-dependent concentration of oxidized product (Fig. S5B).

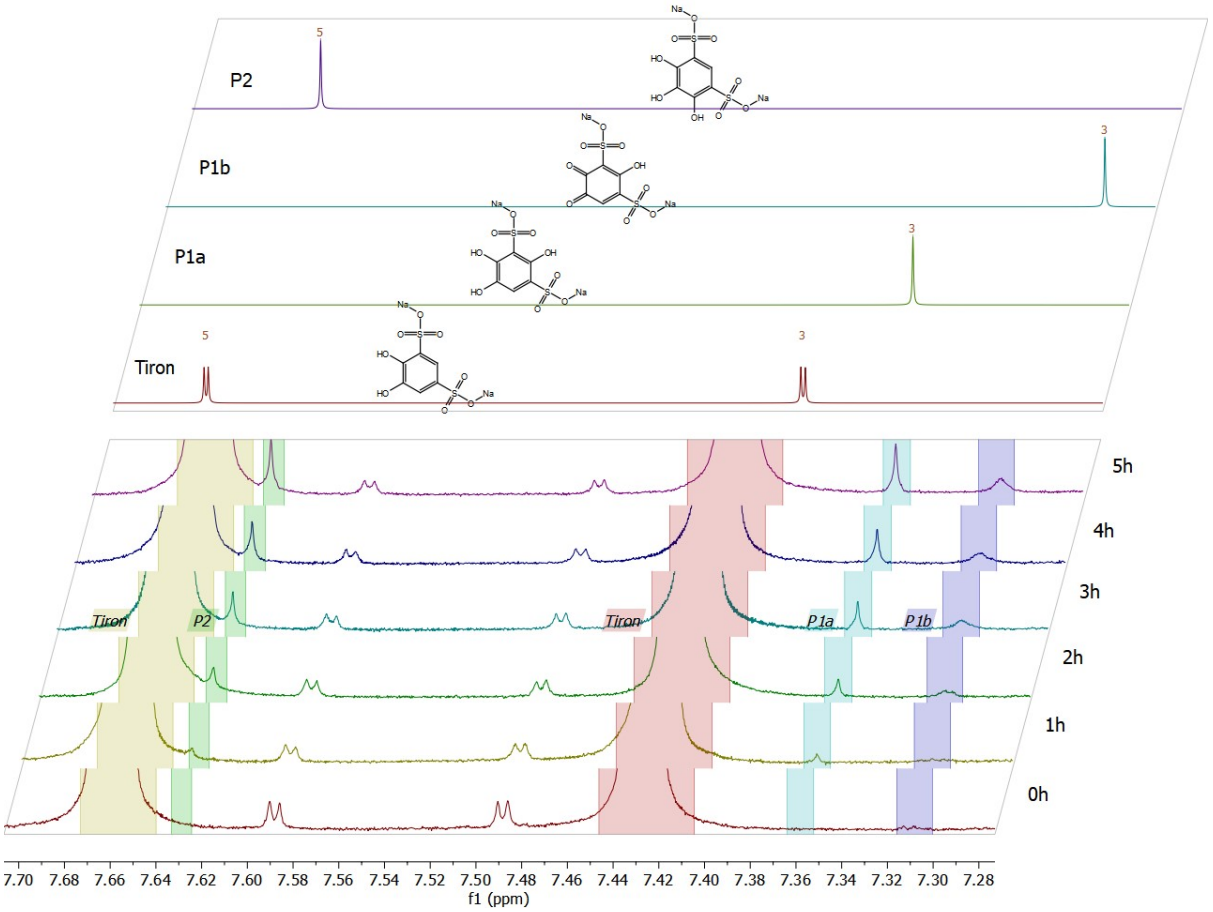

Figure S4. (Top) Model prediction of ^{1}H-NMR spectra of tiron and Michael addition products. (Bottom) ^{1}H NMR spectra of tiron aliquots taken at various times of electrolysis (0.08 mA cm^{-2}; 0.05 M tiron in D_2O). Peak doublets seen at 7.59 & 7.49 ppm corresponds to residual splitting of main tiron peak signals (7.66 & 7.43 ppm)

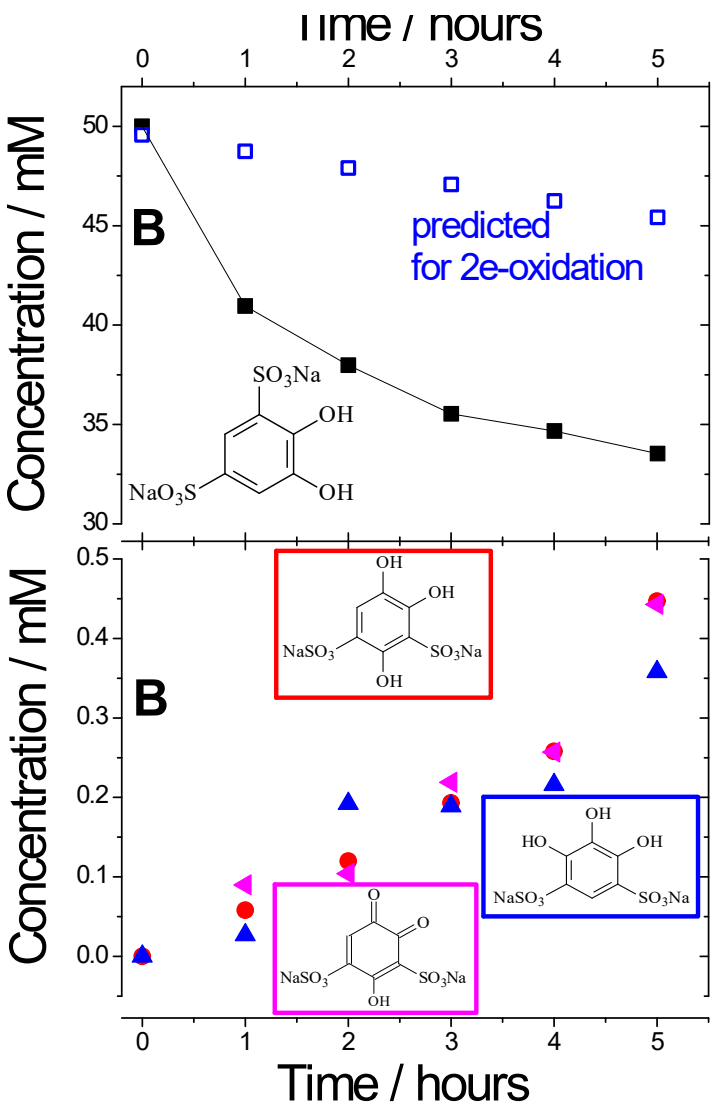

Figure S5. The dependencies of tiron and its oxidation products in pure water on the time of electrolysis (0.08 mA cm^{-2}). **A:** the time decencies of tiron concentrations predicted by Faraday's law for bi-electronic process and measured by ^{1}H NMR (open and filled symbols, respectively); **B:** the time dependencies of the NMR-assayed concentrations of products of tiron oxidation.

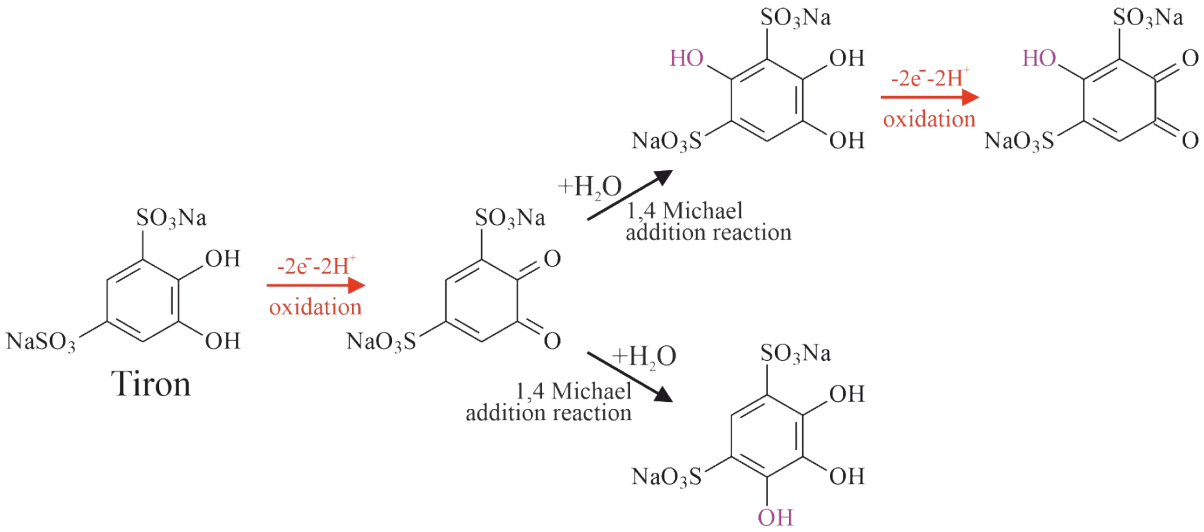

Scheme S1. The scheme of tiron oxidation followed by subsequent 1,4 Michael addition reactions

[1] B. Yang, L. Hoober-Burkhardt, S. Krishnamoorthy, A. Murali, G. K. S. Prakash, S. R. Narayanan, High-performance aqueous organic flow battery with quinone-based redox couples at both electrodes. Journal of The Electrochemical Society 163(7) 2016 A1442-A1449.

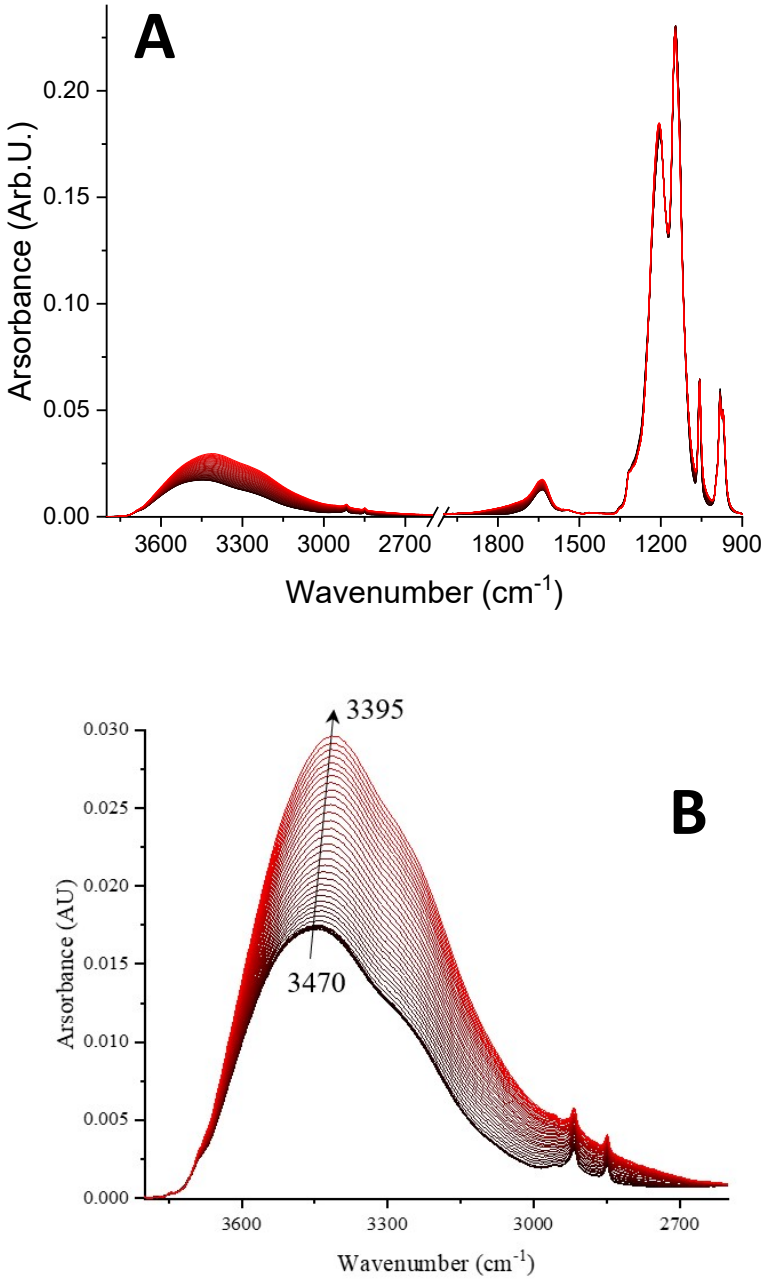

Figure S6. *In-situ* ATR-FTIR under electrolysis conditions. The evolution of ATR-FTIR spectra with elapsed time of electrolysis up to 120 minutes (black (0 min) → red (120 min)) in broad spectral region (**A**) and in O-H vibration region (**B**).

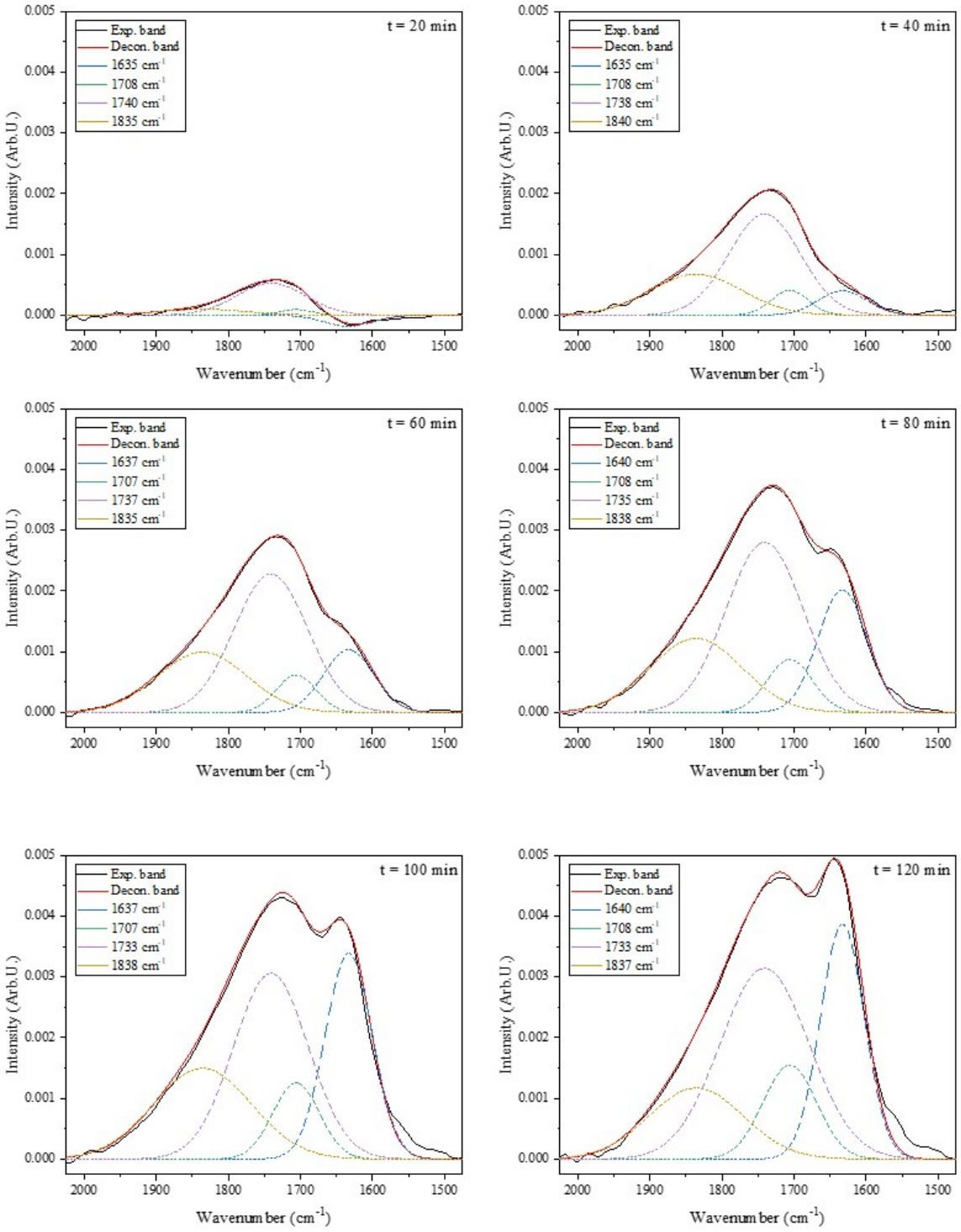

Figure S7. The deconvolution of the band at H-O-H bending region of difference ATR-FTIR spectra collected at different times of electorlysis.

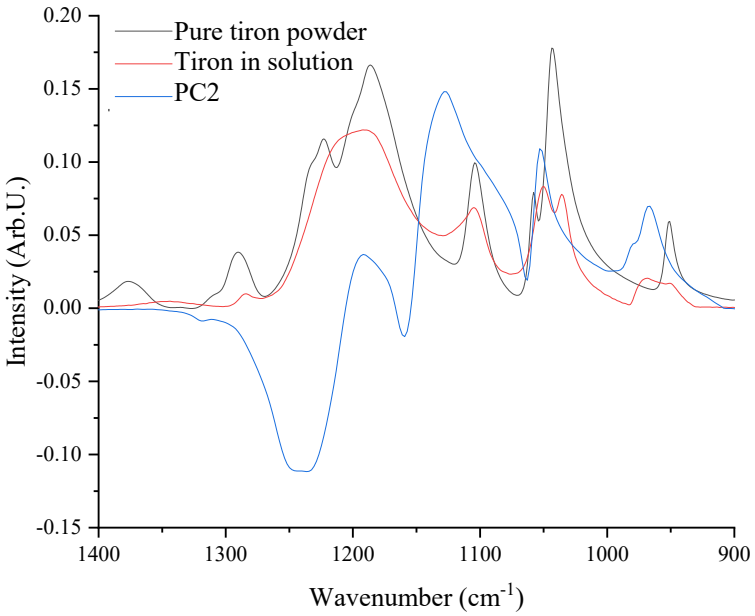

Figure S8. A comparison between the loading spectrum of PC2 and the spectra of pure trion powder and tiron solution.